Article

Signal-On Detection of Caspase-3 with Methylene Blue-Loaded Metal-Organic Frameworks as Signal Reporters

Yaliang Huang [1,2,3,*]**, Jiaqiang Wang** [2]**, Yirui Xu** [1]**, Jiwen Zhang** [2] **and Ning Xia** [2,*]

1   School of Pharmacy, Hunan University of Chinese Medicine, Changsha 410208, China
2   College of Chemistry and Chemical Engineering, Anyang Normal University, Anyang 455000, China; 17838561822@163.com (J.Z.)
3   College of Chemistry and Chemical Engineering, Central South University, Changsha 410083, China
*   Correspondence: yalianghuang@hnucm.edu.cn (Y.H.); ningxia@aynu.edu.cn (N.X.)

Abstract: In this work, we report on an electrochemical method for the signal-on detection of caspase-3 and the evaluation of apoptosis based on the biotinylation reaction and the signal amplification of methylene blue (MB)-loaded metal–organic frameworks (MOFs). Zr-based UiO-66-NH$_2$ MOFs were used as the nanocarriers to load electroactive MB molecules. Recombinant hexahistidine (His$_6$)-tagged streptavidin (rSA) was attached to the MOFs through the coordination interaction between the His$_6$ tag in rSA and the metal ions on the surface of the MOFs. The acetylated peptide substrate Ac-GDEVDGGGPPPPC was immobilized on the gold electrode. In the presence of caspase-3, the peptide was specifically cleaved, leading to the release of the Ac-GDEVD sequence. A N-terminal amine group was generated and then biotinylated in the presence of biotin-NHS. Based on the strong interaction between rSA and biotin, rSA@MOF@MB was captured by the biotinylated peptide-modified electrode, producing a significantly amplified electrochemical signal. Caspase-3 was sensitively determined with a linear range from 0.1 to 25 pg/mL and a limit of detection down to 0.04 pg/mL. Further, the active caspase-3 in apoptosis inducer-treated HeLa cells was further quantified by this method. The proposed signal-on biosensor is compatible with the complex biological samples and shows great potential for apoptosis-related diagnosis and the screening of caspase-targeting drugs.

Keywords: caspase-3; cell apoptosis; metal–organic frameworks; electrochemical biosensor; biotinylation

1. Introduction

Apoptosis is a highly regulated and complicated process of programed cell death for eliminating unwanted cells from tissues and maintaining normal physiological metabolism and tissue homeostasis [1]. The deregulation of apoptosis is closely related to the development of several severe diseases, such as cancers, autoimmune diseases, atherosclerosis, neurological disorder diseases, and so on [2–4]. Thus, the probing of cell apoptosis is essential for clinical investigation and apoptosis-targeted therapy. The progress of apoptosis can be indirectly monitored by measuring the activity of specific intracellular enzymes involved in the apoptotic pathway. Among them, caspases are a family of intracellular cysteine-dependent aspartate-specific proteases which play a critical role in regulating programmed cell death and apoptosis [5,6]. In particular, caspase-3, one of the most frequently activated cysteine proteases during the apoptosis process, has been considered a cellular biomarker of apoptosis [7]. In this aspect, the rapid, sensitive, and selective detection of caspase-3 and the evaluation of apoptosis can provide more important information for disease diagnosis and drug development.

Caspase-3 can specifically recognize and cleave the C terminus of the tetrapeptide motif Asp-Glu-Val-Asp (DEVD). Peptides containing the DEVD motif have been usually used as the substrates or probes for the evaluation of caspase-3 activity and apoptosis [8]. Currently, different analytical techniques have been reported for the detection of

caspase-3 activity, including Western blotting [9], fluorescence [10–12], colorimetry [13–15], surface plasmon resonance spectroscopy [16,17], surface-enhanced Raman scattering spectroscopy [18–20], electrochemistry [21,22], electrochemiluminescence [23–26], and photo-electrochemistry [27,28]. The fluorescence assays are simple and sensitive for monitoring proteolytic events, but they require labor-intensive peptide substrates and specific instrumentation and show relatively low sensitivity [29]. Alternately, electrochemical methods have attracted considerable attention due to their excellent advantages of high sensitivity, rapid response, low cost, and simple operation [30,31]. Therein, diverse forms of voltammetry, such as square wave, differential pulse, linear sweep, and stripping, have been widely used as the electrochemical techniques for the assays of proteases [32,33]. Due to the weak redox activity of amino acids in peptides, the electrical signal generated by the proteolysis was too poor to achieve the sensitive measurement of proteases. For this reason, additional electroactive molecules, enzymes, and nanomaterials were employed as the signal reporters to label the peptide substrates [34,35]. The cleavage of a sequence-specific peptide substrate into two short segments by proteases can cause the release of signal reporters from the electrode surface, leading to the conversion of the proteolysis event into an electrochemical signal. Typically, ferrocene, *p*-nitroaniline, and *p*-methoxyaniline have been conjugated with peptide substrates for the electrochemical detection of caspase-3 activity and cell apoptosis, respectively [36–38]. To further improve sensitivity, Rashidi et al. used horseradish peroxidase-loaded magnetic beads to label the peptide substrate and realized the electrochemical detection of caspase-3 activity during hematopoietic stem cell differentiation [39]. However, the immobilization of a labeled peptide on the solid surface may prevent the interaction between peptide and the active center of proteases due to steric hindrance, thus decreasing enzymatic efficiency [12,40]. To decrease the effect, biotin-labeled peptides could be used as the caspase-3 substrates and streptavidin (SA)-modified materials could be employed to recognize the biotin labels remaining on the electrode surface, such as SA-conjugated alkaline phosphatase [41] and quantum dots-functionalized carbon nanotubes [42]. Additionally, Liu et al. reported an impedimetric biosensor for the determination of caspase-3 activity and cell apoptosis with the self-assembled biotin–phenylalanine network as the signal amplifier [43]. Chen et al. synthesized SA-modified Co_3O_4–Au polyhedra as a signal enhancer to sensitively detect caspase-3 [44]. However, most of these methods are always performed in a signal-off mode, resulting in low signal-to-background ratios.

Alternatively, protease-catalyzed protein/peptide hydrolysis can produce new N termini, and the exposed amino group can serve as a reactive site to be specifically labeled by specific molecules or nanomaterials [45–47]. For instance, biotin-labeled 2-pydidinecarboxyaldehyde was used to selectively react with protein N termini under mild pH and temperature conditions [48,49]. Chen et al. reported an electrochemical method for caspase-3 detection by using *p*-sulfonatocalix [6]arenes sodium-modified graphene oxide to recognize the exposed amine group for the further capture of electroactive methylene blue (MB) via the host–guest interaction [50]. He et al. used citrate-capped silver nanoparticles as electroactive tags to label the generated amine group [51]. However, these nanomaterials are prone to aggregate because of different factors, such as high salt concentration, thiol molecules in samples, or weak intermolecular π–π and Van der Waals interactions. Nanocontainers including liposomes, polymers, and hollow or mesoporous structures are able to entrap small molecules for drug delivery, theranostics, biomedicine, and nanoreactors [52–54]. As an important family of porous crystalline materials, metal–organic frameworks (MOFs) are composed by metal ions/clusters and organic ligands via the coordination interaction [55,56]. Recently, MOFs have been widely used in the development of electrochemical biosensors due to their inherent properties of tunable porous structure, large specific surface area, abundant functional sites, good chemical stability, and excellent biocompatibility [57,58]. The highly ordered pores and large specific surface area endow MOFs with the capability to serve as nanocarriers for signal reporters, such as dyes, redox molecules, enzymes, and nanoparticles. In addition, the abundant coordina-

tively unsaturated metal sites on their external surface can facilitate the self-assembly of hexahistidine (His$_6$)-tagged recombinant biorecognition elements onto the MOF surface via the coordination interactions between the histidine residues in the His$_6$ tags and the metal ions/clusters [59]. In this work, a signal-on electrochemical biosensor for caspase-3 detection was developed by integrating the biotinylation of the exposed amine group with recombinant SA (rSA) and MB-modified MOFs (Scheme 1). Zr-based UiO-66-NH$_2$ MOFs were used as the nanocarriers to load redox-active MB and His$_6$-tagged rSA. After catalyzed cleavage and subsequent biotinylation reactions, rSA@MOF@MB was captured by the biotinylated peptide on the electrode. A large number of MB molecules in MOF could generate an amplified electrochemical signal for sensitive detection of caspase-3 and the monitoring of cell apoptosis with a low limit of detection. The signal-on strategy could be helpful for the diagnosis and prognosis of apoptosis-related diseases and the development of novel protease biosensors.
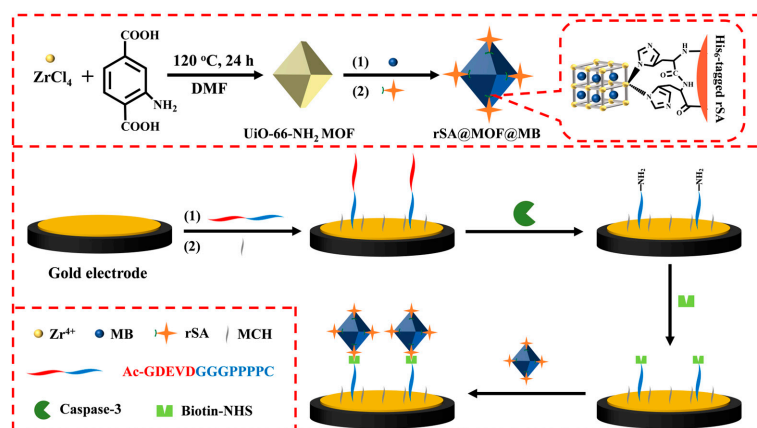
Scheme 1. A schematic illustration of the preparation of rSA@MOF@MB and the principle for the electrochemical detection of caspase-3.

2. Results and Discussion

2.1. Principle of the Method

It has been demonstrated that a spacer module, such as synthetic alkane chains, poly(ethylene glycol) (PEG), and polyproline, is the key to overcoming or reducing the steric hindrance effect between the solid interface and the target [60]. Among them, polyproline, a neutral, compact, and rigid linker, exhibits both good water solubility and hydrophobicity due to the lack of intramolecular hydrogen bonds. More importantly, polyproline can be readily inserted into the peptide during the synthesis process and pattern tight self-assembled monolayers on the solid surface to eliminate non-specific adsorption [61]. Based on this fact, the peptide substrate was designed by connecting the identified DEVD cleavage sequence and the C-terminal cysteine with the linker polyproline (PPPP). The N terminus of the substrate peptide was blocked by an acetyl group, which could not react with the biotinylation reagent biotin-NHS. In the assay, the peptide with a cysteine residue at the C terminus was immobilized on the gold electrode via the robust interaction between Au and the thiol group in cysteine. The acetylated peptide could not react with biotin-NHS due to the absence of a free amino group, and rSA@MOF@MB could not be immobilized on the surface of the peptide-modified electrode. However, in the presence of caspase-3, the cleavage of the peptide by caspase-3 led to the release of acetylated pieces. The exposed amine group could be functionalized with the biotin group in the presence of biotin-NHS. Then, rSA@MOF@MB was captured by the biotinylated peptide-modified electrode surface via the specific binding between rSA and biotin. The differential pulse voltammetry (DPV) current is proportional to the amount of rSA@MOF@MB on the sensing interface, corresponding to the biotinylated peptide, which is dependent on the level and activity of caspase-3.

2.2. Characterization of MOFs

UiO-66-NH$_2$ MOFs were prepared by a conventional solvothermal method and used as the nanocarriers for the accumulation of abundant redox MB molecules due to their high porosity and large surface area [62,63]. The morphologies and structures of UiO-66-NH$_2$ MOF and MOF@MB were characterized by SEM and XRD analyses. As presented in Figure 1A, the as-prepared UiO-66-NH$_2$ MOFs showed a typical octahedron structure with an average size of approximately 170 nm. After the encapsulation of MB, the resulting MOF@MB exhibited similar morphology (Figure 1B). The XRD pattern was further used to characterize the crystal structure of UiO-66-NH$_2$ and MOF@MB. The characteristic peaks are shown in Figure 1C. The results demonstrate that the synthesized UiO-66-NH$_2$ MOF had good morphology, good purity, and high crystallinity, and the encapsulation of MB did not change the morphology and structure of the UiO-66-NH$_2$ MOFs. In addition, the UV–vis spectra of the synthesized MOF materials were collected to confirm the successful encapsulation of the MB molecules. As shown in Figure 1D, there were the absorption peaks at 237 nm and 274 nm in the spectrum of UiO-66-NH$_2$ (red curve) due to the transition of the conjugated π electron of the ligand to the Zr center [64]. After the encapsulation of MB molecules, a new absorption peak at 665 nm in the spectrum of UiO-66-NH$_2$@MB was observed (blue curve), which could be attributed to the n-π* absorption of the MB molecules (black curve) [65]. Further, the color of the MOF powder changed from faint yellow to deep blue (see the inset). In addition, the changes in the BET surface area and pore volume of the MOFs after the encapsulation of MB were investigated. It was found that the BET surface area and pore volume changed from 843 m^2/g and 0.878 cm^3/g to 725 m^2/g and 0.788 cm^3/g, respectively (Figure 2). The above results demonstrate that the MB molecules were successfully entrapped into the UiO-66-NH$_2$ MOFs. To prove that rSA was attached onto the surface of MOF@MB, the change in the Zeta potential of the MOFs was determined. It was found that the Zeta potential of the MOFs changed from 32.8 to 36.1 mV after the entrapment of MB, and changed to 35.2 mV after the attachment of rSA.
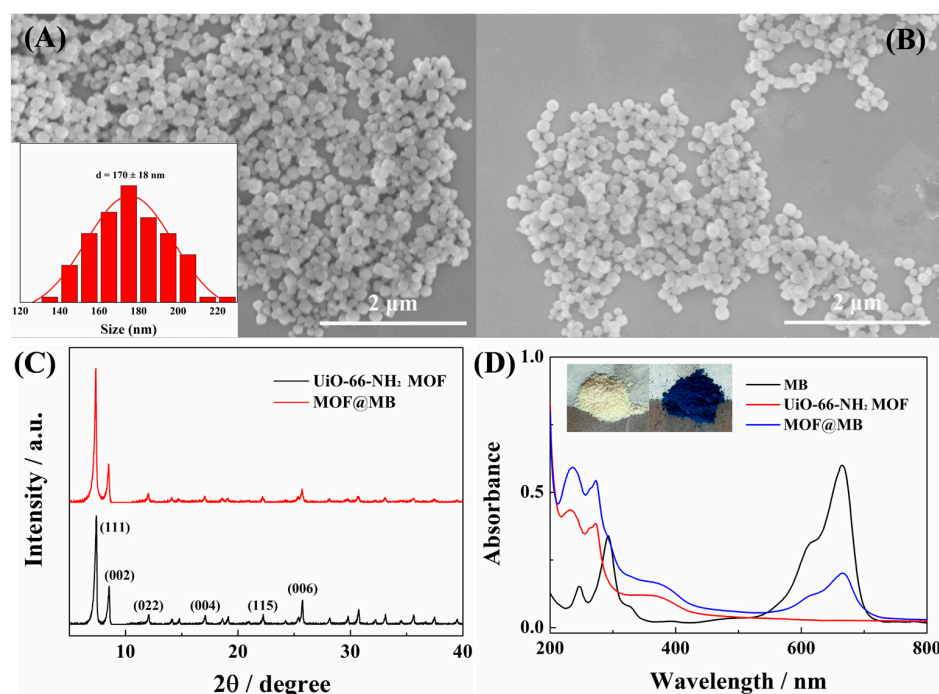

Figure 1. SEM images of (**A**) UiO-66-NH$_2$ MOF and (**B**) MOF@MB. (**C**) XRD patterns of UiO-66-NH$_2$ MOF (black curve) and MOF@MB (red curve). (**D**) UV–vis absorption spectra of MB (black curve), UiO-66-NH$_2$ MOF (red curve), and MOF@MB (blue curve). The inset in panel A shows the size distribution of the UiO-66-NH$_2$ MOF.
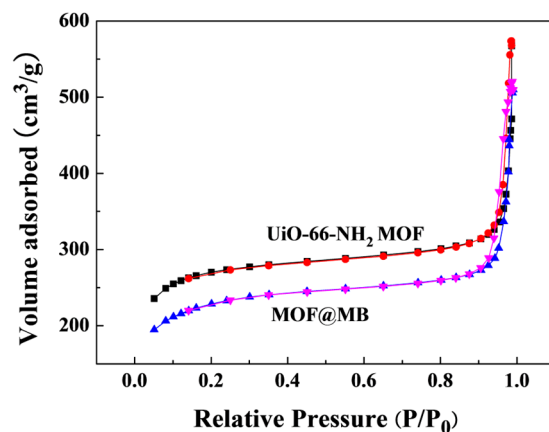
Figure 2. BET analysis of UiO-66-NH$_2$ MOF and MOF@MB.

2.3. Feasibility

Figure 3 shows the DPV responses of the peptide-modified sensing electrode before and after treatment by caspase-3 and follow-up incubation with biotin-NHS and rSA@MOF@MB. In the absence of caspase-3, no voltammetric signal was observed, even when the electrode was incubated with biotin-NHS and rSA@MOF@MB (curve a). The results indicate that the acetylated peptide did not allow for the attachment of biotin-NHS and rSA@MOF@MB on the electrode surface. However, an obviously increased signal was observed when the electrode was treated by caspase-3, biotin-NHS, and rSA@MOF@MB (curve b). This implied that the peptide was cleaved by caspase-3 and the exposed free amino group could be biotinylated for the attachment of rSA@MOF@MB on the electrode surface. Therefore, numerous MB molecules in the MOFs generated a high electrochemical signal. A control experiment was conducted by incubating the caspase-3-treated electrode with rSA@MOF@MB directly, and the electrochemical signal was nearly equal to the blank (curve c), demonstrating that biotinylation is required for the capture of rSA@MOF@MB. These results suggest that the turn-on signal from the captured rSA@MOF@MB was dependent upon the cleavage of peptide by caspase-3 and the biotinylation of the exposed amine group.
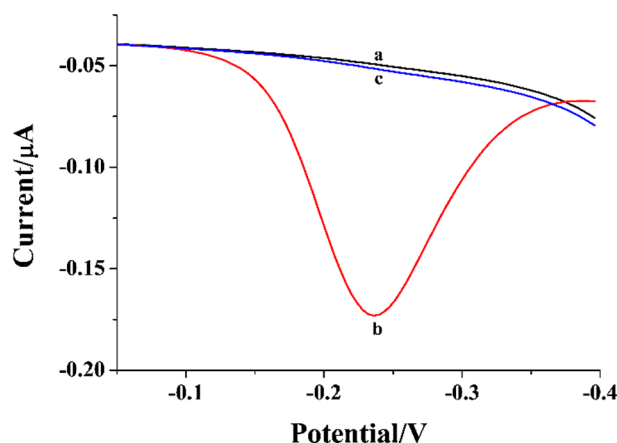

Figure 3. DPV responses corresponding to the peptide-modified sensing electrode after treatment by biotin-NHS + rSA@MOF@MB (**a**), caspase-3 + biotin-NHS + rSA@MOF@MB (**b**), and caspase-3 + rSA@MOF@MB (**c**).

2.4. Optimization of Detection Conditions

To achieve the best detection performance of the method, two important factors were optimized. Appropriate coverage is beneficial for the cleavage of the substrate peptide. Accordingly, the incubation time for peptide immobilization was first optimized. As shown

in Figure 4A, the electrochemical signal increased with the increase in modification time. The current reached the maximum at the modification time of 240 min and began to decline slightly, which is probably due to the steric hindrance from the peptide with high density on the electrode. Thus, 240 min was used as the ideal time for the immobilization of the peptide. We also found that the electrochemical signal was dependent on the proteolysis time (Figure 4B). The current increased and began to level off after 30 min of proteolysis. Therefore, 30 min was selected as the caspase-3 proteolysis time in this study.
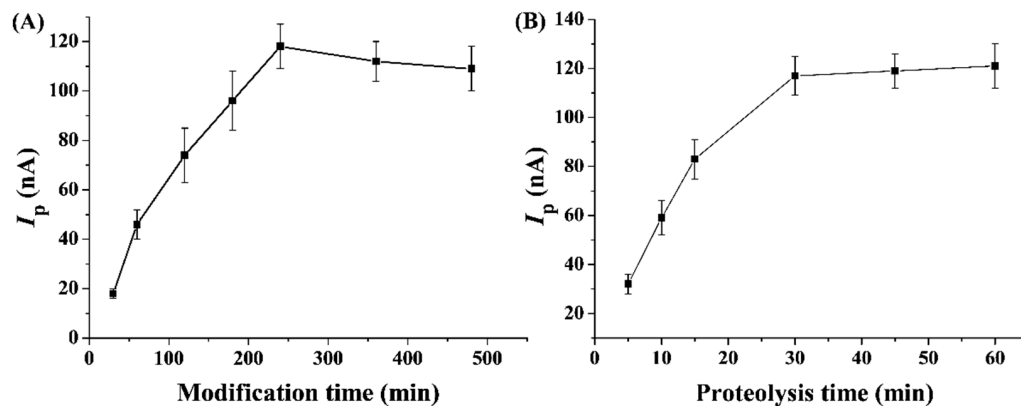

Figure 4. The optimized times for peptide modification (**A**) and proteolysis (**B**).

2.5. Analytical Performance of Method

To ensure the applicability of the method, the prepared biosensors with rSA@MOF@MB as the signal reporters were used to detect different concentrations of caspase-3 under the optimized conditions. As shown in Figure 5A, the DPV signal increased with the increment in caspase-3 concentration from 0 to 100 pg/mL. Notably, the electrochemical signal was negligible without the incubation of caspase-3, demonstrating that the background current and the non-specific adsorption were negligible. There was a good linear relationship between the current and the concentration of caspase-3 in the range from 0.1 to 25 pg/mL. The limit of detection (LOD) was calculated to be 0.04 pg/mL, which was comparable to or even lower than that of other nanomaterial or enzyme-based signal reporters for signal amplification (Table 1). It is noteworthy that the peptide used in this work can ensure high-efficiency proteolysis and high antifouling ability, and the easy preparation and modification of rSA@MOF@MB signal tags simplify the experimental complexity.
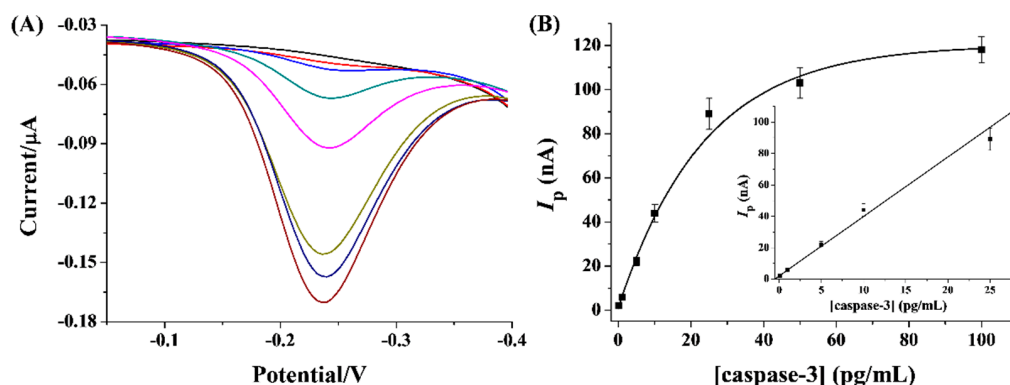

Figure 5. (**A**) DPV responses of the electrochemical biosensor at different concentrations of caspase-3 (from top to bottom: 0, 0.1, 1, 5, 10, 25, 50, and 100 pg/mL). (**B**) The relationship between peak current and caspase-3 concentration. The inset shows the linear portion of the fitting curve.

Table 1. Comparison between proposed method and other electrochemical biosensors for detection of caspase-3.

Signal Labels	Linear Range	LOD	Ref.
MB-carried GO	0.1–100 pg/mL	0.06 pg/mL	[45]
AgNPs	0.5–50 pg/mL	0.1 pg/mL	[51]
HRP-modified magnetic bead	100 pM–1 nM	100 pM	[46]
CB[8]-AgNPs	1–10 ng/mL	24.62 pg/mL	[47]
MB-*p*SC6-GO	10–100 pg/mL	0.0167 pg/mL	[50]
ATCUN-Cu(II) complex	0.5 pg/mL–2 ng/mL	0.2 pg/mL	[8]
biotin-Phe nanoparticle	1–125 pg/mL	1 pg/mL	[43]
AgNPs-modified HeLa cells	0.02–0.2 U/mL	0.02 U/mL	[66]
rSA@MOF@MB	0.1–25 pg/mL	0.04 pg/mL	This work

Abbreviation: SA, streptavidin; MB, methylene blue; AgNPs, silver nanoparticles; HRP, horseradish peroxidase; CB[8], cucurbit[8]uril; pSC_6, *p*-Sulfonatocalix[6]arenes sodium; ATCUN, amino terminal Cu(II) and Ni(II)-binding motif; Phe, phenylalanine.

2.6. Selectivity of Method and Evaluation of Inhibition Viability

To evaluate the specificity of the method for caspase-3 detection, the biosensor was incubated with BSA and two proteases (thrombin and trypsin) as interfering substances. Under the same experimental conditions, the DPV currents for the assays of these samples were collected. As illustrated in Figure 6, the currents for the non-targets were close to that of the blank control. The result suggests that the proposed method had an excellent selectivity toward caspase-3. In addition, we found that the current for the detection of caspase-3 was 92% of the original value after the storage of rSA@MOF@MB at 4 °C for three months, indicating that the signal reporters exhibited good stability.
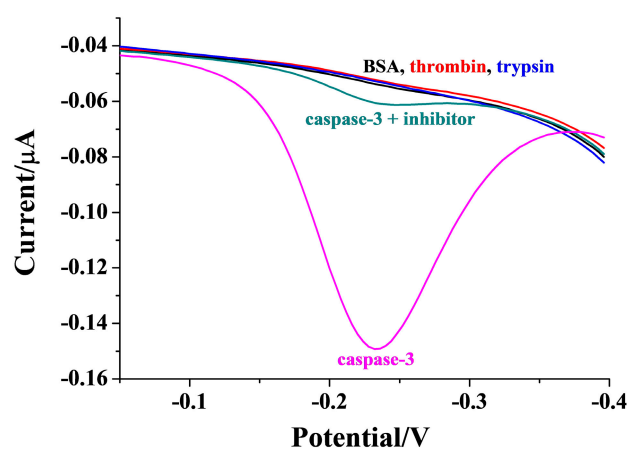

Figure 6. DPV responses of the electrochemical biosensor for the detection of different samples. The concentrations of caspase-3, inhibitor, BSA, thrombin, and trypsin were 25 pg/mL, 50 pM, 10 ng/mL, 1 ng/mL, and 1 ng/mL, respectively.

To demonstrate that the signal change was attributed to the enzymatic activity of caspase-3, DEVD-FMK was used to inhibit the activity of caspase-3. As a result, the current in the presence of DEVD-FMK was remarkably lower than that without the addition of inhibitor. Moreover, the responses exhibited a dependence on the inhibitor concentration (Figure 7), suggesting that the signal change arose from the catalytic activity of caspase-3. From the corresponding relationship between the inhibition viability of DEVD-FMK for caspase-3 and the inhibitor concentration, the half-maximum inhibition value (IC_{50}) was found to be about 6.8 pM. The value is in good agreement with that determined by other methods [8,43], indicating that the biosensor has the potential to screen potential inhibitors as therapeutic drugs.
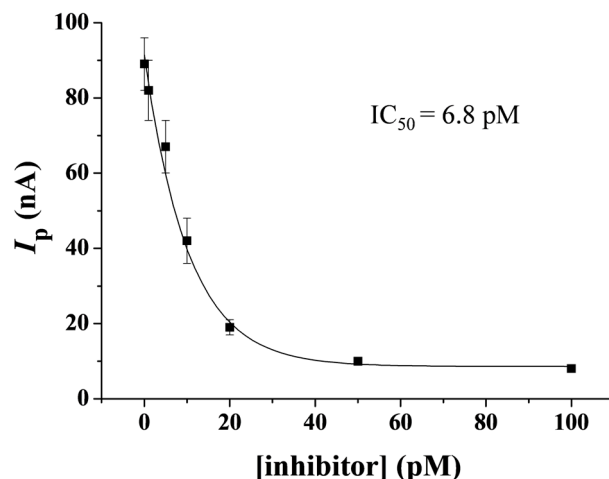
Figure 7. The relationship between peak current and inhibitor concentration for the assay of 25 pg/mL caspase-3.

2.7. Assays of Caspase-3 in HeLa Cells

To evaluate the analytical reliability and applicability, the developed biosensor was employed to monitor drug-induced cell apoptosis. In this work, HeLa cells were used as the model cell type for apoptosis and treated with STS, a commonly used apoptosis inducer. At the same time, a control group was prepared with the same cell concentration without incubation with STS. As presented in Figure 8, a small current was observed in the control group, indicating that caspase-3 was inactive in HeLa cells. However, a significant increase in the current was observed when the cells were treated with STS, demonstrating that caspase-3 in the apoptotic cells was activated to efficiently cleave the peptide. Moreover, the current increased significantly with the increase in the number of apoptotic HeLa cells, which further confirmed the practicability and effectiveness of the designed biosensor for apoptosis evaluation.
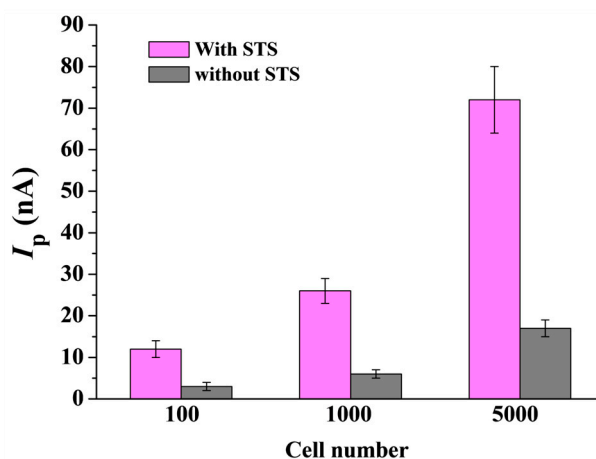
Figure 8. The relationship between peak current and cell number for the assays of caspase-3 in HeLa cells with and without treatment by STS.

3. Materials and Methods

3.1. Chemicals and Reagents

Zirconium chloride ($ZrCl_4$), MB, and benzoic acid were supplied by Titan Co. Ltd. (Shanghai, China). Aminoterephthalic acid (NH_2-BDC), 6-mercapto-1-hexanol (MCH), and tris(2-carboxyethyl)phosphine hydrochloride (TCEP) were provided by Sigma-Aldrich (Shanghai, China). Caspase-3 was purchased from New England BioLabs (Ipswich, MA, USA). Glucose oxidase, trypsin, thrombin, *β*-secretase, and Dulbecco's modified Eagle's

medium (DMEM) were provided by Sangon Biotech. Co., Ltd. (Shanghai, China). Staurosporine (STS) and other reagents were obtained from Aladdin Company (Shanghai, China). The peptide with the sequence Ac-GDEVDGGGPPPPC was synthesized and purified by Synpeptides Co., Ltd. (Shanghai, China). All regents in the experiment were of analytical grade, and all the stock solutions were prepared with ultrapure water (18.2 MΩ/cm) from a Millipore water purification system.

3.2. Apparatus

Electrochemical measurements were conducted on a CHI 660E electrochemical workstation (Shanghai, China). The three-electrode system consisted of a gold (Au) electrode as the working electrode, a Ag/AgCl electrode (immersed in saturated KCl solution) as the reference electrode, and a Pt wire as the auxiliary electrode. The UV–vis spectra were recorded on a spectrophotometer (Cary 60; Agilent, Santa Clara, CA, USA). The morphological analysis was performed with scanning electron microscopy (SEM) equipment. The phase constituents of the MOFs were characterized by an Ultima III X-ray diffraction (XRD) apparatus. The N_2 adsorption–desorption experiments were conducted at 77 K on a Micromeritics Gemini VII surface area and porosity instrument (Norcross, GA, USA). The Zeta potential of the MOFs was determined by a Nano ZS90 particle size analyzer.

3.3. Preparation of rSA@MOF@MB

The UiO-66-NH_2 MOFs were prepared according to the previously reported work [62]. In detail, $ZrCl_4$ (0.120 g), NH_2-BDC (0.110 g), and benzoic acid (1.9 g) were dissolved in 10 mL of DMF, and the mixture was treated with sonication for 10 min. Then, the solution was transferred into a Teflon-lined autoclave and placed in an oven at 120 °C for 24 h. After that, the solution was cooled to room temperature, and the product was collected by centrifugation at 8000 rpm for 10 min and then washed with DMF and ethanol three times, respectively. Finally, the precipitates were dried at 60 °C under vacuum overnight.

The UiO-66-NH_2 MOFs were used to carry MB molecules based on the reported literature [63]. Briefly, the as-synthesized pale yellow UiO-66-NH_2 MOFs (25 mg) were dispersed in 25 mL of water with the aid of sonication for 15 min. Next, MB (2.5 mg) was added to the solution, which was stirred for 24 h at room temperature. The final solid was collected by centrifugation at 8000 rpm for 10 min and washed with water thoroughly. The prepared MOF@MB samples were dried for further use.

The assembly of rSA on the MOFs was achieved based on metal–His_6 coordination interactions [59,67]. MOF@MB (0.1 mg/mL) was dispersed in the phosphate buffer (10 mM, pH 7.4) and then mixed with the rSA solution (50 μg/mL). After mild shaking at room temperature for 1 h, the suspension was centrifuged at 8000 rpm for 10 min, and the solid was washed with the buffer several times. The obtained rSA@MOF@MB was stored at 4 °C for further use.

3.4. Electrode Modification

The Au electrode was treated by a fresh piranha solution consisting of H_2SO_4 and 30% H_2O_2 in a volume ratio of 3:1 for approximately 10 min. After being rinsed thoroughly with ultrapure water, the electrode was polished with 0.05 μm alumina slurry and washed ultrasonically in 50% ethanol for a few seconds. After that, the electrode was scanned in 0.5 M H_2SO_4 for 10 circles with a scan rate of 0.1 V/s and a potential range from –0.3 to 1.6 V. After having been cleaned with ultrapure water and dried in N_2 atmosphere, the Au electrode was incubated with the phosphate buffer (10 mM, pH 7.4) containing 10 μM peptide and 0.5 mM TCEP at 4 °C and washed with the buffer. Then, the peptide-modified electrode was immersed into a 1 mM MCH solution for 1 h to block the unreacted sites and reduce non-specific adsorption. The resulting sensing electrode was washed with ethanol and water for further use.

3.5. Electrochemical Detection of Caspase-3

The peptide-modified sensing electrode was incubated with HEPES buffer (10 mM, pH 7.4) containing a given concentration of caspase-3 at room temperature for a given time. After having been washed with water, the electrode was immersed into the DMF solution containing 0.1 mM biotin-NHS. After reacting for 15 min, the electrode was washed and further incubated with 0.01 mg/mL rSA@MOF@MB suspension for 10 min; then, the electrode was washed thoroughly and subjected to electrochemical measurement in the Tris-HCl buffer solution (20 mM, pH 7.4) containing 0.1 M NaCl. For inhibitor evaluation, the experiment was performed by using the same procedure, except that caspase-3 was replaced with a mixture of DEVD-FMK and caspase-3.

3.6. Cell Culture and Apoptosis Assays

The procedures for cell culture and the preparation of cell lysates followed our previous report [43]. Briefly, HeLa cells were incubated in Dulbecco's modified Eagle's medium (DMEM) supplemented with 10% fetal calf serum. They were then cultured at 37 °C in a humidified atmosphere with 5% CO_2 for 1 day. The tested inducer STS was added to induce apoptosis. After incubation for 8 h, the cells were washed and lysed with the ice-cold lysis buffer. Next, 0.5 mL of the lysate was transferred to a centrifuge tube and centrifuged at 12,000 rpm for 10 min at 4 °C. The supernatant was collected and diluted with assay buffer for the assays. Caspase-3 in the diluted lysate was analyzed by following the aforementioned procedure.

4. Conclusions

In summary, we developed an electrochemical biosensor for the signal-on detection of caspase-3 and the evaluation of cell apoptosis based on the biotinylation reaction and multifunctional MOFs. UiO-66-NH$_2$ MOFs served as the nanocarriers to load electroactive MB molecules and as the platforms to anchor rSA proteins through the interactions between His$_6$ tags and metal ions. The exposed amino group generated from caspase-3 proteolysis was first biotinylated and further reacted with rSA@MOF@MB via the biotin–rSA interactions. The developed electrochemical biosensor showed a good linear range and a low LOD for caspase-3 detection. Furthermore, this method was used to evaluate inhibition efficiency and drug-induced cell apoptosis, providing a new signal amplification strategy for protease assays in clinical applications.

References

1. Hengartner, M.O. The biochemistry of apoptosis. *Nature* **2000**, *407*, 770–776. [CrossRef]
2. Favaloro, B.; Allocati, N.; Graziano, V.; Di Ilio, C.; De Laurenzi, V. Role of apoptosis in disease. *Aging* **2012**, *4*, 330–349. [CrossRef]
3. Roos, W.P.; Kaina, B. DNA damage-induced cell death: From specific DNA lesions to the DNA damage response and apoptosis. *Cancer Lett.* **2013**, *332*, 237–248. [CrossRef] [PubMed]
4. Carneiro, B.A.; El-Deiry, W.S. Targeting apoptosis in cancer therapy. *Nat. Rev. Clin. Oncol.* **2020**, *17*, 395–417. [CrossRef]

5.   Shalini, S.; Dorstyn, L.; Dawar, S.; Kumar, S. Old, new and emerging functions of caspases. *Cell Death Differ.* **2015**, *22*, 526–539. [CrossRef] [PubMed]

6.   Julien, O.; Wells, J.A. Caspases and their substrates. *Cell Death Differ.* **2017**, *24*, 1380–1389. [CrossRef]

7.   Buckley, C.D.; Pilling, D.; Henriquez, N.V.; Parsonage, G.; Threlfall, K.; Scheel-Toellner, D.; Simmons, D.L.; Akbar, A.N.; Lord, J.M.; Salmon, M. RGD peptides induce apoptosis by direct caspase-3 activation. *Nature* **1999**, *397*, 534–539. [CrossRef] [PubMed]

8.   Deng, D.; Hao, Y.; Yang, S.; Han, Q.; Liu, L.; Xiang, Y.; Tu, F.; Xia, N. A signal-on electrochemical biosensor for evaluation of caspase-3 activity and cell apoptosis by the generation of molecular electrocatalysts on graphene electrode surface for water oxidation. *Sens. Actuat. B Chem.* **2019**, *286*, 415–420. [CrossRef]

9.   Ji, C.; Amarnath, V.; Pietenpol, J.A.; Marnett, L.J. 4-hydroxynonenal induces apoptosis via caspase-3 activation and cytochrome c release. *Chem. Res. Toxicol.* **2001**, *14*, 1090–1096. [CrossRef]

10.   Liu, L.; Li, X.; Zhang, H.; Chen, H.; Abualrejal, M.M.A.; Song, D.; Wang, Z. Six-in-one peptide functionalized upconversion@polydopamine nanoparticle-based ratiometric fluorescence sensing platform for real-time evaluating anticancer efficacy through monitoring caspase-3 activity. *Sens. Actuat. B Chem.* **2021**, *333*, 129554–129561. [CrossRef]

11.   Shen, Y.; Xin, Z.; Zhu, Y.; Wang, J. Mesoporous carbon nanospheres featured multifunctional fluorescent nanoprobe: Simultaneous activation and tracing of caspase-3 involved cell apoptosis. *Sens. Actuat. B Chem.* **2022**, *358*, 131485–131493. [CrossRef]

12.   Ma, X.; Lv, Y.; Liu, P.; Hao, Y.; Xia, N. Switch-on fluorescence analysis of protease activity with the assistance of a nickel ion-nitrilotriacetic acid-conjugated magnetic nanoparticle. *Molecules* **2023**, *28*, 3426. [CrossRef]

13.   Gurtu, V.; Kain, S.R.; Zhang, G. Fluorometric and colorimetric detection of caspase activity associated with apoptosis. *Anal. Biochem.* **1997**, *251*, 98–102. [CrossRef] [PubMed]

14.   Pan, Y.; Guo, M.; Nie, Z.; Huang, Y.; Peng, Y.; Liu, A.; Qing, M.; Yao, S. Colorimetric detection of apoptosis based on caspase-3 activity assay using unmodified gold nanoparticles. *Chem. Commun.* **2012**, *48*, 997–999. [CrossRef] [PubMed]

15.   Zhou, Z.; Peng, L.; Wang, X.; Xiang, Y.; Tong, A. A new colorimetric strategy for monitoring caspase 3 activity by HRP-mimicking DNAzyme-peptide conjugates. *Analyst* **2014**, *139*, 1178–1183. [CrossRef]

16.   Yuan, X.; Niu, Z.; Liu, L.; Zeng, Y.; Ma, L.; Nie, Z.; Tian, Z.; Kai, D.; Zhang, F.; Liu, G.; et al. Intensity interrogation-based high-sensitivity surface plasmon resonance imaging biosensor for apoptosis detection in cancer. *Biosensors* **2023**, *13*, 946. [CrossRef]

17.   Zhu, H.; Mao, Z.; Chen, J.; Hu, J.; Hu, X.; Koh, K.; Chen, H. Cucurbit[7]urils induced bimetallic nanoparticles network for ultra-sensitive detection of Caspase-3 based on surface plasmon resonance. *Microchem. J.* **2021**, *171*, 106792–106799. [CrossRef]

18.   Choi, J.H.; El-Said, W.A.; Choi, J.-W. Highly sensitive surface-enhanced Raman spectroscopy (SERS) platform using core/double shell (Ag/polymer/Ag) nanohorn for proteolytic biosensor. *Appl. Surf. Sci.* **2020**, *506*, 144669–144674. [CrossRef]

19.   Zhu, W.; Wang, C.-Y.; Hu, J.-M.; Shen, A.-G. Promoted "Click" SERS detection for precise intracellular imaging of caspase-3. *Anal. Chem.* **2021**, *93*, 4876–4883. [CrossRef]

20.   Zhuang, Y.; Dong, H.; Liu, T.; Zhao, Y.; Xu, Y.; Zhao, X.; Sun, D. Highly sensitive and selective SERS detection of caspase-3 during cell apoptosis based on the target-induced hotspot effect. *Analyst* **2024**, *149*, 490–496. [CrossRef]

21.   Yu, J.; Yang, A.; Wang, N.; Ling, H.; Song, J.; Chen, X.; Lian, Y.; Zhang, Z.; Yan, F.; Gu, M. Highly sensitive detection of caspase-3 activity based on peptide-modified organic electrochemical transistor biosensors. *Nanoscale* **2021**, *13*, 2868–2874. [CrossRef]

22.   Shin, J.H.; Gul, A.R.; Hyun, M.S.; Choi, C.H.; Park, T.J.; Park, J.P. Electrochemical detection of caspase-3 based on a chemically modified M13 phage virus. *Bioelectrochemistry* **2022**, *145*, 108090–108097. [CrossRef]

23.   Dong, Y.P.; Chen, G.; Zhou, Y.; Zhu, J.J. Electrochemiluminescent Sensing for Caspase-3 Activity Based on Ru(bpy)$_3{}^{2+}$-Doped Silica Nanoprobe. *Anal. Chem.* **2016**, *88*, 1922–1929. [CrossRef]

24.   Cheng, M.; Zhou, J.; Zhou, X.; Xing, D. Peptide cleavage induced assembly enables highly sensitive electrochemiluminescence detection of protease activity. *Sens. Actuat. B Chem.* **2018**, *262*, 516–521. [CrossRef]

25.   Liang, G.-X.; Zhao, K.-R.; He, Y.-S.; Liu, Z.-J.; Ye, S.-Y.; Wang, L. Carbon dots and gold nanoparticles doped metal-organic frameworks as high-efficiency ECL emitters for monitoring of cell apoptosis. *Microchem. J.* **2021**, *171*, 106787–106793. [CrossRef]

26.   Luo, W.; Chu, H.; Wu, X.; Ma, P.; Wu, Q.; Song, D. Disposable biosensor based on novel ternary Ru-PEI@PCN-333(Al) self-enhanced electrochemiluminescence system for on-site determination of caspase-3 activity. *Talanta* **2021**, *239*, 123083–123090. [CrossRef] [PubMed]

27.   Yang, R.; Li, Y.; Zou, K.; Meng, L.; Zhang, X.; Chen, J. A label-free and blocker-free photoelectrochemical strategy for highly sensitive caspase-3 assay. *Chem. Commun.* **2018**, *54*, 4830–4833. [CrossRef] [PubMed]

28.   Wang, Z.; Liu, J.; Liu, X.; Shi, X.; Dai, Z. Photoelectrochemical approach to apoptosis evaluation via multi-functional peptide- and electrostatic attraction-guided excitonic response. *Anal. Chem.* **2019**, *91*, 830–835. [CrossRef]

29.   Bachor, R. Peptidyl-resin substrates as a tool in the analysis of caspase activity. *Molecules* **2022**, *27*, 4107. [CrossRef]

30.   Hung, V.W.S.; Veloso, A.J.; Chow, A.M.; Ganesh, H.V.S.; Seo, K.; Kendüzler, E.; Brown, I.R.; Kerman, K. Electrochemical impedance spectroscopy for monitoring caspase-3 activity. *Electrochim. Acta* **2015**, *162*, 79–85. [CrossRef]

31.   Liu, G.; Li, Y.; Liu, M.; Cheng, J.; Yang, S.; Gao, F.; Liu, L. Overview on peptide-based electrochemical biosensors. *Int. J. Electrochem. Sci.* **2023**, *18*, 100395–100413. [CrossRef]

32.   Li, H.Y.; Qi, H.J.; Chang, J.F.; Gai, P.P.; Li, F. Recent progress in homogeneous electrochemical sensors and their designs and applications. *TrAC-Trend. Anal. Chem.* **2022**, *156*, 116712–116726. [CrossRef]

33.   Eivazzadeh-Keihan, R.; Saadatidizaji, Z.; Maleki, A.; de la Guardia, M.; Mahdavi, M.; Barzegar, S.; Ahadian, S. Recent progresses in development of biosensors for thrombin detection. *Biosensors* **2022**, *12*, 767. [CrossRef]

34. Karimzadeh, A.; Hasanzadeh, M.; Shadjou, N.; Guardia, M.D.L. Peptide based biosensors. *TrAC-Trend. Anal. Chem.* **2018**, *107*, 1–20. [CrossRef]
35. Yuan, L.; Liu, L. Peptide-based electrochemical biosensing. *Sens. Actuat. B Chem.* **2021**, *344*, 130232–130257. [CrossRef]
36. Xiao, H.; Liu, L.; Meng, F.; Huang, J.; Li, G. Electrochemical approach to detect apoptosis. *Anal. Chem.* **2008**, *80*, 5272–5275. [CrossRef]
37. Takano, S.; Shiomoto, S.; Inoue, K.Y.; Ino, K.; Shiku, H.; Matsue, T. Electrochemical approach for the development of a simple method for detecting cell apoptosis based on caspase-3 activity. *Anal. Chem.* **2014**, *86*, 4723–4728. [CrossRef]
38. Sixiang, S.; Inoue, K.Y.; Shiomoto, S.; Takano, S.; Ino, K.; Shiku, H.; Matsue, T. Amperometric detection of apoptosis by using *p*-methoxyaniline-conjugated substrate for caspase-3. *ChemElectroChem* **2017**, *4*, 941–946. [CrossRef]
39. Khalilzadeh, B.; Charoudeh, H.N.; Shadjou, N.; Mohammad-Rezaei, R.; Omidi, Y.; Velaei, K.; Aliyari, Z.; Rashidi, M.-R. Ultrasensitive caspase-3 activity detection using an electrochemical biosensor engineered by gold nanoparticle functionalized MCM-41: Its application during stem cell differentiation. *Sens. Actuat. B Chem.* **2016**, *231*, 561–575. [CrossRef]
40. Gao, F.; Liu, G.; Qiao, Y.; Dong, X.; Liu, L. Streptavidin-conjugated DNA for the boronate affinity-based detection of poly(ADP-ribose) polymerase-1 with improved sensitivity. *Biosensors* **2023**, *13*, 723. [CrossRef]
41. Zhou, S.; Wang, Y.; Zhao, M.; Jiang, L.P.; Zhu, J.J. CdSeTe@CdS@ZnS Quantum-Dot-Sensitized Macroporous TiO$_2$ Film: A Multisignal-Amplified Photoelectrochemical Platform. *Chemphyschem* **2015**, *16*, 2826–2835. [CrossRef] [PubMed]
42. Zhang, J.J.; Zheng, T.T.; Cheng, F.F.; Zhu, J.J. Electrochemical sensing for caspase 3 activity and inhibition using quantum dot functionalized carbon nanotube labels. *Chem. Commun.* **2011**, *47*, 1178–1180. [CrossRef] [PubMed]
43. Xia, N.; Huang, Y.; Cui, Z.; Liu, S.; Deng, D.; Liu, L.; Wang, J. Impedimetric biosensor for assay of caspase-3 activity and evaluation of cell apoptosis using self-assembled biotin-phenylalanine network as signal enhancer. *Sens. Actuat. B Chem.* **2020**, *320*, 128436–128442. [CrossRef]
44. Yang, R.; Zou, K.; Li, Y.; Meng, L.; Zhang, X.; Chen, J. Co$_3$O$_4$-Au polyhedra: A multifunctional signal amplifier for sensitive photoelectrochemical assay. *Anal. Chem.* **2018**, *90*, 9480–9486. [CrossRef]
45. Chen, H.; Zhang, J.; Gao, Y.; Liu, S.; Koh, K.; Zhu, X.; Yin, Y. Sensitive cell apoptosis assay based on caspase-3 activity detection with graphene oxide-assisted electrochemical signal amplification. *Biosens. Bioelectron.* **2015**, *68*, 777–782. [CrossRef]
46. Khalilzadeh, B.; Shadjou, N.; Eskandani, M.; Charoudeh, H.N.; Omidi, Y.; Rashidi, M.-R. A reliable self-assembled peptide based electrochemical biosensor for detection of caspase 3 activity and apoptosis. *RSC Adv.* **2015**, *5*, 58316–58326. [CrossRef]
47. Song, S.; Hu, X.; Li, H.; Zhao, J.; Koh, K.; Chen, H. Guests involved CB[8] capped silver nanoparticles as a means of electrochemical signal enhancement for sensitive detection of Caspase-3. *Sens. Actuat. B Chem.* **2018**, *274*, 54–59. [CrossRef]
48. MacDonald, J.I.; Munch, H.K.; Moore, T.; Francis, M.B. One-step site-specific modification of native proteins with 2-pyridinecarboxyaldehydes. *Nat. Chem. Biol.* **2015**, *11*, 326–331. [CrossRef]
49. Song, X.; Ren, X.; Mei, Q.; Liu, H.; Huang, H. Advancing in-depth N-terminomics detection with a cleavable 2-pyridinecarboxyaldehyde probe. *J. Am. Chem. Soc.* **2024**, *146*, 6487–6492. [CrossRef]
50. Song, S.; Shang, X.; Zhao, J.; Hu, X.; Koh, K.; Wang, K.; Chen, H. Sensitive and selective determination of caspase-3 based on calixarene functionalized reduction of graphene oxide assisted signal amplification. *Sens. Actuat. B Chem.* **2018**, *267*, 357–365. [CrossRef]
51. Fan, H.; Kou, J.; Han, D.; Li, P.; Zhang, D.; Wu, Q.; He, Q. Sensitive proteolysis assay based on the detection of a highly characteristic solid-state process. *RSC Adv.* **2015**, *5*, 48893–48897. [CrossRef]
52. Hofmann, C.; Duerkop, A.; Baeumner, A.J. Nanocontainers for analytical applications. *Angew.Chem. Int. Ed.* **2019**, *58*, 12840–12860. [CrossRef] [PubMed]
53. Zhao, J.; Dang, Z.; Muddassir, M.; Raza, S.; Zhong, A.; Wang, X.; Jin, J. A new type Co(II)-based photocatalyst for the nitrofurantoin antibiotic degradation. *J. Mol. Struct.* **2024**, *1312*, 138501.
54. Zhao, J.; Dang, Z.; Muddassir, M.; Raza, S.; Zhong, A.; Wang, X.; Jin, J. A new Cd(II)-based coordination polymer for efficient photocatalytic removal of organic dyes. *Molecules* **2023**, *28*, 6848. [CrossRef] [PubMed]
55. Luo, D.; Huang, J.; Jian, Y.; Singh, A.; Kumar, A.; Liu, D.; Pan, Y.; Ouyang, Q. Metal–organic frameworks (MOFs) as apt luminescent probes for the detection of biochemical analytes. *J. Mater. Chem. B* **2023**, *11*, 6802–6822. [CrossRef] [PubMed]
56. He, T.; Kong, X.-J.; Li, J.-R. Chemically stable metal-organic frameworks: Rational construction and application expansion. *Acc. Chem. Res.* **2021**, *54*, 3083–3094. [CrossRef] [PubMed]
57. Liu, S.; Lai, C.; Liu, X.; Li, B.; Zhang, C.; Qin, L.; Huang, D.; Yia, H.; Zhang, M.; Li, L.; et al. Metal-organic frameworks and their derivatives as signal amplification elements for electrochemical sensing. *Coord. Chem. Rev.* **2020**, *424*, 213520. [CrossRef]
58. Chang, Y.; Lou, J.; Yang, L.; Liu, M.; Xia, N.; Liu, L. Design and application of electrochemical sensors with Metal-organic frameworks as the electrode materials or signal tags. *Nanomaterials* **2022**, *12*, 3248. [CrossRef] [PubMed]
59. Roder, R.; Preiss, T.; Hirschle, P.; Steinborn, B.; Zimpel, A.; Hohn, M.; Radler, J.O.; Bein, T.; Wagner, E.; Wuttke, S.; et al. Multifunctional nanoparticles by coordinative self-assembly of His-tagged units with metal-organic frameworks. *J. Am. Chem. Soc.* **2017**, *139*, 2359–2368. [CrossRef]
60. Jin, Z.; Ling, C.; Li, Y.; Zhou, J.; Li, K.; Yim, W.; Yeung, J.; Chang, Y.C.; He, T.; Cheng, Y.; et al. Spacer matters: All-peptide-based ligand for promoting interfacial proteolysis and plasmonic coupling. *Nano Lett.* **2022**, *22*, 8932–8940. [CrossRef]
61. Nowinski, A.K.; Sun, F.; White, A.D.; Keefe, A.J.; Jiang, S. Sequence, structure, and function of peptide self-assembled monolayers. *J. Am. Chem. Soc.* **2012**, *134*, 6000–6005. [CrossRef]

62. Sun, Z.; Wu, S.; Ma, J.; Shi, H.; Wang, L.; Sheng, A.; Yin, T.; Sun, L.; Li, G. Colorimetric sensor array for human semen identification designed by coupling Zirconium metal-organic frameworks with DNA-modified gold nanoparticles. *ACS Appl. Mater. Interfaces* **2019**, *11*, 36316–36323. [CrossRef] [PubMed]

63. Sun, Z.; Wang, L.; Wu, S.; Pan, Y.; Dong, Y.; Zhu, S.; Yang, J.; Yin, Y.; Li, G. An electrochemical biosensor designed by using Zr-based metal-organic frameworks for the detection of glioblastoma-derived exosomes with practical application. *Anal. Chem.* **2020**, *92*, 3819–3826. [CrossRef] [PubMed]

64. Long, J.; Wang, S.; Ding, Z.; Wang, S.; Zhou, Y.; Huang, L.; Wang, X. Amine-functionalized zirconium metal-organic framework as efficient visible-light photocatalyst for aerobic organic transformations. *Chem. Commun.* **2012**, *48*, 11656–11658. [CrossRef] [PubMed]

65. Helal, A.; Qamaruddin, M.; Aziz, M.A.; Shaikh, M.N.; Yamani, Z.H. MB-UiO-66-NH$_2$ metal-organic framework as chromogenic and fluorogenic sensor for hydrazine gydrate in aqueous solution. *ChemistrySelect* **2017**, *2*, 7630–7636. [CrossRef]

66. Wu, D.; He, Y.; Tong, L.; Wang, J.; Liu, L.; Yi, X.; Hu, S. Electrochemical determination of caspase-3 using signal amplification by HeLa cells modified with silver nanoparticles. *Microchim. Acta* **2021**, *188*, 110–117. [CrossRef] [PubMed]

67. Wei, B.; Xu, H.; Cheng, L.; Yuan, Q.; Liu, C.; Gao, H.; Liang, H. Highly selective entrapment of His-tagged enzymes on superparamagnetic Zirconium-based MOFs with robust renewability to enhance pH and thermal stability. *ACS Biomater. Sci. Eng.* **2021**, *7*, 3727–3736. [CrossRef]